



Structural and Mössbauer spectroscopic study of hexagonal Laves-phase $Zr(Fe_xCr_{1-x})_2$ alloys and their hydrides

J.A.H. Coaquira^a, H.R. Rechenberg^{a,*}, J. Mestnik Filho^b

^aInstituto de Física, Universidade de São Paulo, CP 66318, 05315-970 São Paulo, Brazil

^bInstituto de Pesquisas Energéticas e Nucleares, CP 11049, 05422-970 São Paulo, Brazil

Received 15 February 1999

Abstract

Hexagonal (C14) Laves-phase $Zr(Fe_xCr_{1-x})_2$ alloys with $x=0.3, 0.4, 0.5, 0.6$ and 0.7 have been prepared by arc melting and the corresponding hydrides have been formed by hydrogen uptake at 1 atm pressure. X-ray diffractograms have been measured and analyzed with the Rietveld method. ^{57}Fe Mössbauer spectra, measured at room temperature, could be fitted with two doublets with 3:1 area ratio, corresponding to the two Fe sites in the C14 structure. The quadrupole splitting (Δ) and isomer shift (δ) dependences on x are discussed in terms of volume and charge effects. The hydrides showed volume expansions of up to 22% without any crystal structure change. Both Mössbauer hyperfine parameters Δ and δ increased markedly in the hydrides as compared to the alloys. Tetrahedral hole radii have been calculated from measured crystalline parameters and their relationship to hydrogen site preferences is discussed. © 1999 Elsevier Science S.A. All rights reserved.

Keywords: Laves phases; Iron alloys; Metal hydrides; Mössbauer spectroscopy

1. Introduction

Zirconium-based Laves phase compounds with transition metals have attracted a great deal of attention owing to their high hydrogen storage capability [1]. In addition to their technological potential, such materials raise questions of fundamental interest concerning the effect of hydrogen absorption on their structural, electronic and magnetic properties. The Laves-phase structures also provide a convenient framework for investigating phenomena such as the onset of magnetism, chemical disorder effects, etc. as a function of transition metals concentration. Mössbauer spectroscopy is particularly suited to investigate such effects in Fe-containing materials. While extensive magnetic and Mössbauer studies have been devoted to $Zr(Fe_xM_{1-x})_2$ pseudobinary alloys with $M=Co$ [2], Al [2,3] and Mn [4], the Cr alloys have received much less attention. To our knowledge, only one Mössbauer characterization of the $Zr(Fe_xCr_{1-x})_2$ system in the full composition range has been reported [5].

While the end compounds $ZrFe_2$ and $ZrCr_2$ crystallize in the C15 cubic structure, the $Zr(Fe_xCr_{1-x})_2$ pseu-

dobinaries exhibit the C14 hexagonal structure in the $x \approx 0.2-0.8$ concentration range [6]. In this work we report crystallographic and Mössbauer hyperfine data for a series of hexagonal $Zr(Fe_xCr_{1-x})_2$ alloys and for the corresponding hydrides, obtained by charging each alloy to its maximum hydrogen absorption capacity at normal pressure. X-ray diffraction data were analyzed to yield cell parameters and metal-atom position parameters. Only Mössbauer results at room temperature will be presented here; low-temperature data will be reported in a forthcoming paper in connection with the magnetic properties of these materials.

2. Experimental details

$Zr(Fe_xCr_{1-x})_2$ samples with $x=0.3, 0.4, 0.5, 0.6$ and 0.7 were prepared by melting the elements in an arc furnace under argon atmosphere. The purity of the initial elements was: Zr (99.95%), Fe (99.98%) and Cr (99.997%). The samples were remelted several times to ensure good homogeneity. No further heat treatment was done after melting.

The hydrogen charging was carried out in a Sievert-type facility at a pressure of ~ 1 atm of high purity hydrogen

*Corresponding author. Tel.: +55-11-8186877; fax: +55-11-8186984.

E-mail address: hercilio@macbeth.if.usp.br (H.R. Rechenberg)

(99.999%). Finely pulverized samples were activated by heating in vacuum at 800°C and exposed to hydrogen gas while cooling down slowly to room temperature. After that, the samples were cooled to the liquid nitrogen temperature, the hydrogen gas was removed and air was introduced into the reactor at 0.4 atm for about 2 h. In this process the surfaces of the finely grounded samples react slowly with oxygen, thus preventing them from burning when exposed to air at ambient or higher temperature. The absorbed hydrogen amount was determined for each sample by measuring its mass increase.

The crystallographic characterization was performed by X-ray diffraction using CuK α radiation. The diffractograms were obtained in the $20^\circ < 2\theta < 90^\circ$ range with 0.05° steps and were analyzed with the Rietveld refinement method. The quantitative phase analysis was carried out using the Hill and Howard relation [7]. Mössbauer spectra were obtained at room temperature using a $^{57}\text{Co}(\text{Rh})$ source and the isomer shift data are quoted with respect to $\alpha\text{-Fe}$.

3. Results and discussion

3.1. X-ray diffraction

3.1.1. Alloys

The X-ray diffraction data were refined with the C14-hexagonal structure (space group $P6_3/mmc$) assuming a statistical distribution of Fe and Cr atoms at both crystallographic sites (2a and 6h), in accordance with neutron powder diffraction results obtained by Canet et al. [8]. Fig. 1 shows the pattern refined for the sample with $x=0.3$. Additional weak reflections were observed and were found to be due to $\alpha\text{-Zr}$; quantitative phase analysis yielded about 1% of this phase. In the present work we did not observe any peaks in the diffraction patterns that could be ascribed

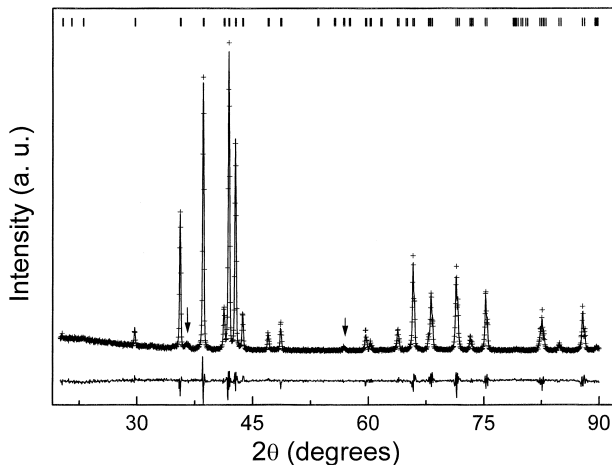


Fig. 1. Refined powder diffractogram of $\text{Zr}(\text{Fe}_{0.3}\text{Cr}_{0.7})_2$. Arrows indicate $\alpha\text{-Zr}$ reflections.

Table 1

Structural parameters of $\text{Zr}(\text{Fe}_x\text{Cr}_{1-x})_2$ alloys obtained from X-ray powder diffraction Rietveld analysis (Space group $P6_3/mmc$)

x_{Fe}	a (Å)	c (Å)	x	z	R_{wp} (%)
0.3	5.0495(7)	8.2849(3)	0.8295(7)	0.0644(3)	12.5
0.4	5.0373(2)	8.2655(3)	0.8289(9)	0.0634(3)	14.5
0.5	5.0282(2)	8.2475(4)	0.8305(8)	0.0636(2)	12.5
0.6	5.0191(2)	8.2254(5)	0.8314(10)	0.0628(3)	14.6
0.7	5.0089(2)	8.2030(4)	0.8303(8)	0.0626(3)	12.7

to layer stacking defects as suggested by Mestnik et al. for the ZrCr_2 compound [9]. It is believed that such defects arise only when the compounds are prepared with excess of Cr/Fe instead of Zr as in the present case.

Table 1 summarizes the structural parameters obtained from the Rietveld refinement for these alloys. Cell parameters decrease linearly with increasing Fe concentration and agree well with recent neutron diffraction data [8].

Detailed analysis of the neighborhood of A and B atoms for the AB_2 Laves phases with C14-structure indicates that there are eight different first-neighbor interatomic distances: two d_{AA} , three d_{AB} and three d_{BB} distances [10]. The latter result disagrees with that given in Ref. [11] where only two d_{BB} distances are quoted. We have used our data to estimate the 2a and 6h site radii, defined as one-half the average nearest-neighbor distance. It was found (Fig. 2) that r_{2a} is consistently larger than r_{6h} by about 0.6%. These radii would be equal if the lattice

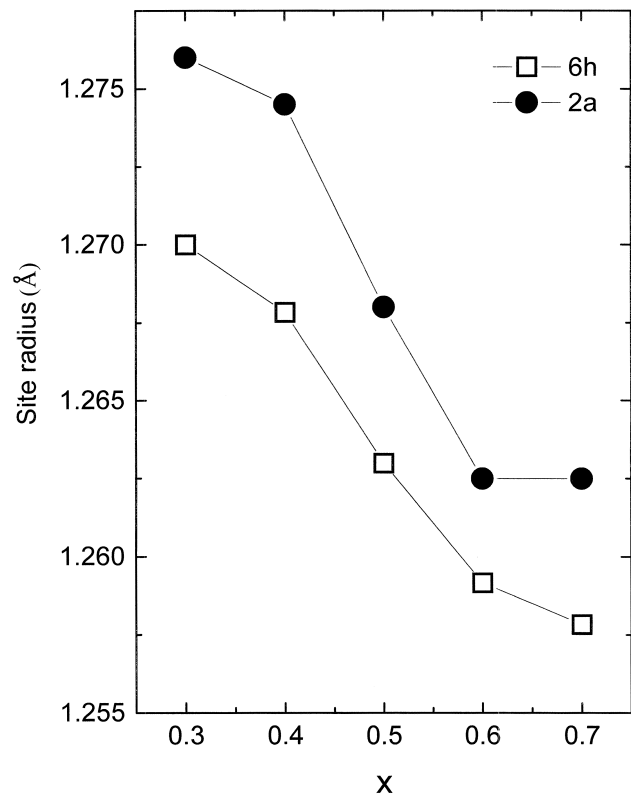


Fig. 2. 2a and 6h site radii against Fe concentration.

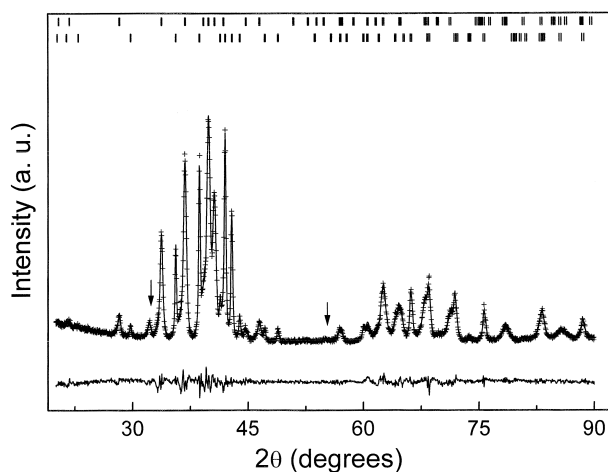


Fig. 3. Refined powder diffractogram of $Zr(Fe_{0.7}Cr_{0.3})_2H_{2.5}$. Arrows indicate Zr hydride reflections.

parameters had the ideal values $x=5/6$, $z=1/16$ and $c/a=(8/3)^{1/2}$.

3.1.2. Hydrides

The hexagonal structure of the metal sublattice remains unchanged upon the hydrogen uptake. In samples with Fe concentration $x \geq 0.5$, two phases were observed to coexist: one with a very low hydrogen content (α phase) as inferred from their lattice constants, very similar to those of the hydrogen-free alloys, and a hydrogen-rich one (β phase) characterized by an expanded lattice. In addition, a small amount of tetragonal Zr hydride [12] was also detected. Fig. 3 shows a diffractogram of the $Zr(Fe_{0.7}Cr_{0.3})_2$ hydride fitted with these phases. The α phase volume fraction was 30% for the latter sample, but did not exceed 2% for $x=0.5$ and 0.6. The α -phase lattice constants were 0.3–0.4% larger than for the corresponding unhydrided alloy, indicating that small H amounts were dissolved in the lattice.

The structural parameters for the hydride phases are listed in Table 2, as well as the hydrogen content and the fractional lattice volume increase after H absorption. It can be seen that the absorbed hydrogen amount at a fixed gas pressure of ~ 1 atm decreases for increasing Fe concentration. These results are consistent with those obtained by Shaltiel et al. [1]. The relative volume expansion was

proportional to n_H within experimental error, at the rate $(d \ln V / d n_H) = 0.059(1)$.

Absorbed hydrogen in AB_2 Laves phases may occupy one or more of three types of tetrahedral interstices, denoted as B4, AB3 and A2B2 according to their corner atom types. Many theoretical and experimental studies (see e.g. [13,14]) have indicated that A2B2 sites are predominantly occupied, AB3 less frequently, and B4 never. In the present work we have no direct evidence for hydrogen occupancy since X-rays do not probe H atoms, but a neutron diffraction analysis on $Zr(Fe_xCr_{1-x})_2D_n$ carried out by Canet et al. [8] has shown that only A2B2 interstices were occupied. An earlier study on $ZrCr_2D_n$ [15] has yielded similar results, except for n approaching the limiting value 3.5 at which some deuterium also entered AB3 sites.

Westlake [16] stressed the importance of volume effects in determining site occupancies in hydrides and proposed a simple rule, according to which a tetrahedral hole in a stable hydride can only hold a hydrogen atom if its radius is larger than 0.4 Å. Using our experimental data we have calculated hole radii r_h in order to check Westlake's criterion for our samples¹. A2B2 sites are of four types: $6h_2$, $12k_2$, $24l$ and $6h_1$ (listed in order of decreasing H occupancy as determined by Canet et al. [8]), and AB3 sites are either $4f$ or $12k_1$. The calculated r_h for all types of interstitials are shown in Fig. 4 for both alloys (open symbols) and hydrides (full symbols).

As can be observed in Fig. 4, in the hydrides all four types of A2B2 sites have hole radii greater than 0.4 Å, thus fulfilling Westlake's criterion for hydrogen occupancy. The smallest radii correspond to $6h_1$ sites, which also show [8] the smallest occupation probability. A2B2 holes are largest also in the pure alloys, where at least some have $r_h > 0.33$ Å. The latter figure is quoted by Westlake [16] as being the smallest hole radius capable of holding a H atom in solid solution (α phase), though not in a stable hydride (β phase). B4 (4e) holes, on the other hand, are clearly seen to be much too small in any case.

AB3 holes exhibit an unexpected behavior: while $12k_1$ -type holes are rather small, straddling the 0.4 Å limit, $4f$

¹The hole size r_h is defined as the radius of the largest sphere that can be in contact with four atomic spheres centered at specified positions. Atomic radii used were [16] $r_{Zr} = 1.602$ Å at A sites and weighted averages of $r_{Fe} = 1.274$ Å, $r_{Cr} = 1.282$ Å at B sites.

Table 2

Structural parameters of $Zr(Fe_xCr_{1-x})_2H_n$ compounds derived from X-ray powder diffraction patterns. Space group $P6_3/mmc$. The number n_H of absorbed H atoms/f.u. and the volume expansion upon H uptake are also indicated

x_{Fe}	n_H	a (Å)	c (Å)	x	z	$\Delta V/V$ (%)	R_{wp} (%)
0.3	3.6	5.3895(2)	8.7970(4)	0.8390(7)	0.0645(2)	20.9	10.3
0.4	3.7	5.3962(2)	8.8125(3)	0.8376(9)	0.0648(2)	22.4	8.7
0.5	3.3	5.3438(4)	8.7101(4)	0.8408(9)	0.0642(3)	19.3	11.1
0.6	3.0	5.3114(3)	8.6543(6)	0.8410(7)	0.0643(2)	17.8	9.9
0.7	2.5	5.2798(4)	8.6044(9)	0.8391(9)	0.0643(3)	16.6	8.8

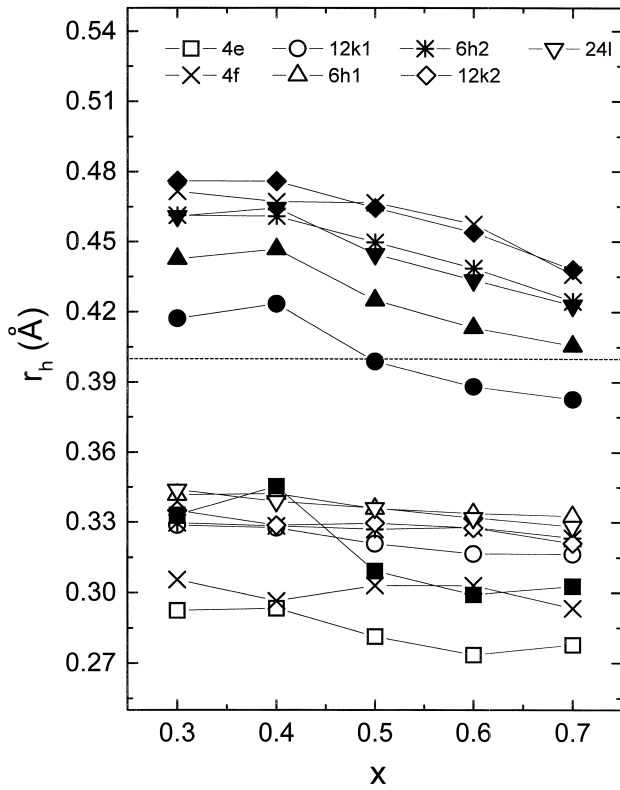


Fig. 4. Tetrahedral hole radii for A2B2 (6h₂, 12k₂, 24l, 6h₁), AB3 (4f, 12k₁) and B4 (4e) sites. Open symbols: alloys, filled symbols: hydrides. Dashed line at $r_h = 0.40$ Å indicates Westlake's minimum radius for hydrogen occupancy.

holes are comparable in size to the largest A2B2 ones. Thus, from pure size considerations some AB3 occupancy would be allowed in these hydrides, contrary to neutron diffraction evidence. It is apparent that, for this specific site, Westlake's rule is overridden by another effect – most likely, the “Shoemaker exclusion rule” [13] which states that two tetrahedra with a face in common cannot be simultaneously occupied. Since a 4f tetrahedron shares faces with three 12k₂ tetrahedra, at least one of which is certainly occupied (occupation probability is ~ 0.3 according to [8]), the exclusion rule will apply. As to the reason why 12k₂ sites are preferred in the first place, it may be thought that, other factors being equal, H atoms will choose an environment with fewer Fe neighbors: indeed, the H absorption capacity is vanishingly small for ZrFe₂ [1].

3.2. Mössbauer spectroscopy

3.2.1. Alloys

The room-temperature Mössbauer spectra of the Zr(Fe_xCr_{1-x})₂ alloys, shown in Fig. 5, could be fitted with two quadrupolar doublets with areas constrained to the 3:1 ratio, consistent with a random Fe occupancy of the 6h and 2a sites. Such a spectral decomposition could actually be done in two distinct ways, denoted as fits I and II.

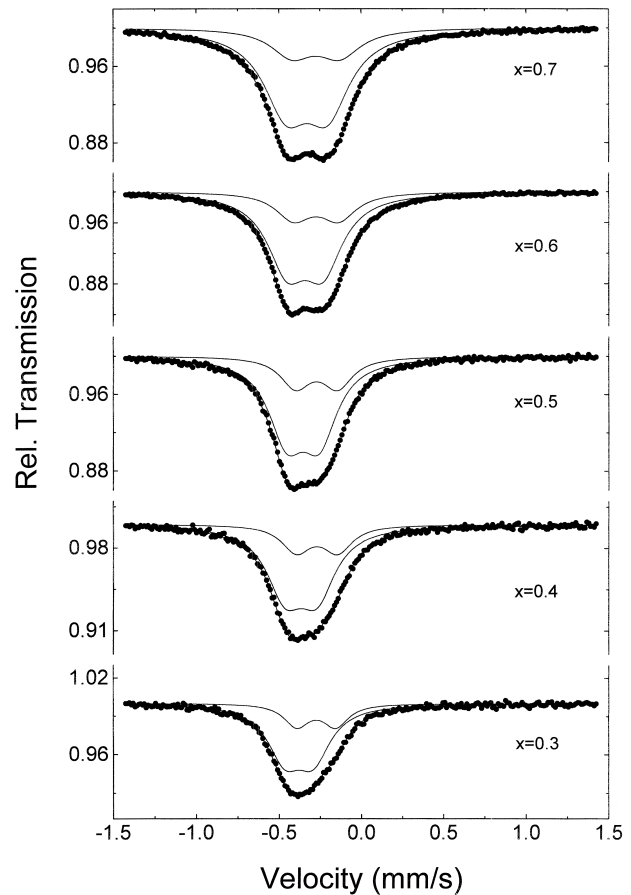


Fig. 5. Room-temperature Mössbauer spectra of Zr(Fe_xCr_{1-x})₂ alloys fitted with two doublets in the 3:1 ratio.

According to fit I, a larger quadrupole splitting Δ and a less negative isomer shift δ resulted for site 6h than for site 2a, while the reverse occurred for fit II. Since both fits had equivalent statistical quality for all spectra, we made an assignment based on a nearest-neighbor point-charge model estimate of the electric field gradient (EFG) at both Fe sites. Fig. 6 depicts the close neighborhood of an Fe atom at 2a and 6h sites, respectively. All nearest-neighbor sites are either 2a or 6h, randomly occupied by Fe or Cr atoms. The EFG tensor was calculated using the experimentally determined atomic positions and was numerically diagonalized, yielding the quadrupole splitting Δ up to an arbitrary factor. As a result, Δ was found to be 20% larger at 2a than at 6h; this result is consistent with fit II, which was thus chosen as the correct one. It is noteworthy that the opposite result is expected if one loosely considers the 6h neighborhood to be “more distorted” than that of 2a, as Fig. 6 tends to suggest. Close inspection, however, shows that two out-of-plane neighbors to 6h atoms are close to the angle $\theta = \cos^{-1}(1/\sqrt{3})$ with respect to the EFG principal z axis, so they contribute little to V_{zz} .

The fitted parameters are summarized in Table 3. As shown in Fig. 7, the fitted Δ values increase nearly linearly with Fe concentration. The lattice contraction upon Fe

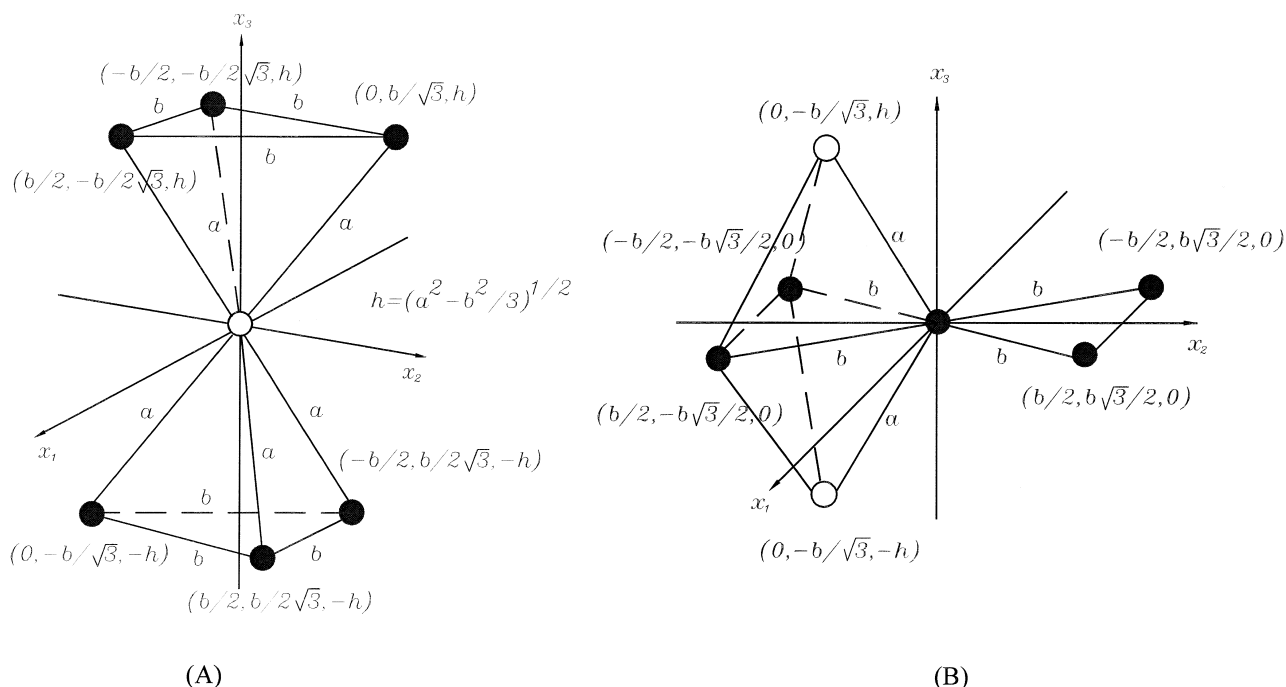


Fig. 6. First-neighbor atomic environment of (A) 2a site and (B) 6h site. Cartesian axes shown are local principal axes of the EFG tensor, to which indicated atomic coordinates are referred.

substitution accounts, through the $(1/R^3)$ factor of the EFG, only for a small fraction of the observed Δ vs. x dependence. This result implies a significant charge difference between Fe and Cr atoms. If one adheres to the nearest-neighbor point-charge model to provide a simple picture, the data can be reasonably well described (see Fig. 7) by assuming an average charge $q_{av} = xq_{Fe} + (1-x)q_{Cr}$ with $q_{Fe} = +0.30e$ and $q_{Cr} = +0.16e$ (Sternheimer factor $\gamma_{\infty} = -9$, nuclear quadrupole moment $Q(^{57}\text{Fe}) = 0.2$ b).

Isomer shift data are shown in Fig. 8. It is seen that $\delta(2a)$ is less negative than $\delta(6h)$, which is consistent with the larger atomic volume of the former sites, as indicated in Section 3.1.1. On the other hand, δ does not decrease for decreasing cell volume (i.e. for increasing x), in contrast to similar systems such as $\text{Zr}(\text{Fe}_x\text{Al}_{1-x})_2$ [2,3] and

$\text{Zr}(\text{Fe}_x\text{Mn}_{1-x})_2$ [4]. This suggests that for the present system electron transfer effects predominate over the usual volume effect and have the opposite sign. If we assume both effects to be additive, i.e.

$$\frac{d\delta}{dx} = \left(\frac{d\delta}{dx}\right)_{\text{vol}} + \left(\frac{d\delta}{dx}\right)_{\text{el}} = \left(\frac{\partial\delta}{\partial\ln V}\right) \cdot \left(\frac{d\ln V}{dx}\right) + \left(\frac{d\delta}{dx}\right)_{\text{el}}$$

and further assume $\partial\delta/\partial\ln V \approx 1.33$ mm s⁻¹ as for α -Fe [17], our results yield $(\partial\delta/\partial x)_{\text{el}} = 0.15$ and 0.22 mm s⁻¹ for 2a and 6h Fe sites, respectively. It was theoretically found by Ivey and Northwood [14] that charge transfer from Zr to Fe should increase for increasing x in $\text{Zr}(\text{Fe}_x\text{Cr}_{1-x})_2$; the positive sign of $(\partial\delta/\partial x)_{\text{el}}$ is consistent with this result if it is assumed that transferred electrons

Table 3

Fitted parameters from Mössbauer spectra: quadrupolar splitting Δ , isomer shift δ , and linewidth Γ ^a

x	n_{H}	6h site			2a site		
		Δ (mm s ⁻¹)	δ (mm s ⁻¹)	Γ (mm s ⁻¹)	Δ (mm s ⁻¹)	δ (mm s ⁻¹)	Γ (mm s ⁻¹)
0.3	0	0.176(2)	-0.264(1)	0.255(4)	0.237(3)	-0.159(2)	0.200(6)
0.3	3.6	0.496(3)	0.182(2)	0.287(4)	0.422(3)	0.251(4)	0.200(*)
0.4	0	0.194(2)	-0.251(1)	0.275(2)	0.250(4)	-0.155(3)	0.233(8)
0.4	3.7	0.463(2)	0.204(2)	0.307(4)	0.429(3)	0.284(2)	0.192(4)
0.5	0	0.199(2)	-0.239(1)	0.267(3)	0.256(4)	-0.157(3)	0.242(6)
0.5	3.3	0.465(2)	0.145(1)	0.339(4)	0.392(3)	0.222(2)	0.200(*)
0.6	0	0.218(1)	-0.226(1)	0.288(2)	0.272(4)	-0.159(3)	0.288(5)
0.6	3.0	0.441(1)	0.103(1)	0.323(4)	0.385(3)	0.190(2)	0.200(*)
0.7	0	0.252(1)	-0.215(2)	0.325(3)	0.288(6)	-0.160(6)	0.351(10)
0.7	2.5	0.455(2)	0.079(2)	0.309(1)	0.390(13)	0.184(6)	0.222(3)

^a Uncertainties in parentheses refer to least significant digits. (*) indicates the parameter was kept fixed.

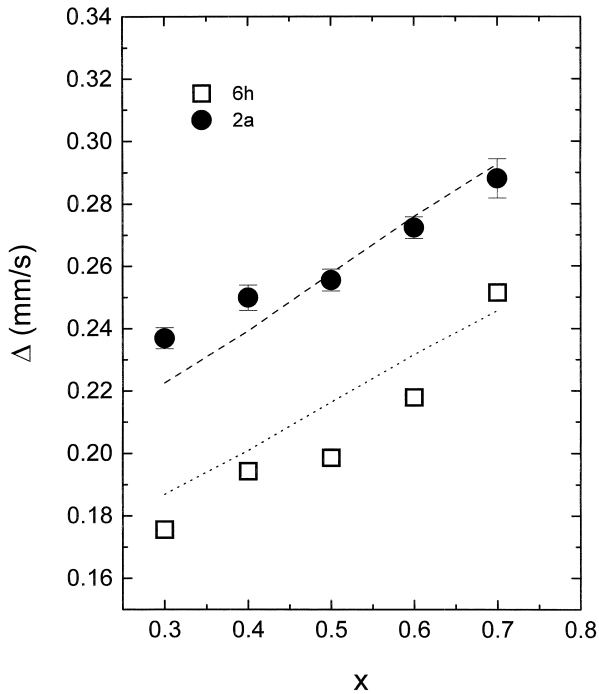


Fig. 7. Experimental quadrupole splittings of $Zr(Fe_xCr_{1-x})_2$. Dashed lines show calculated values according to point-charge model.

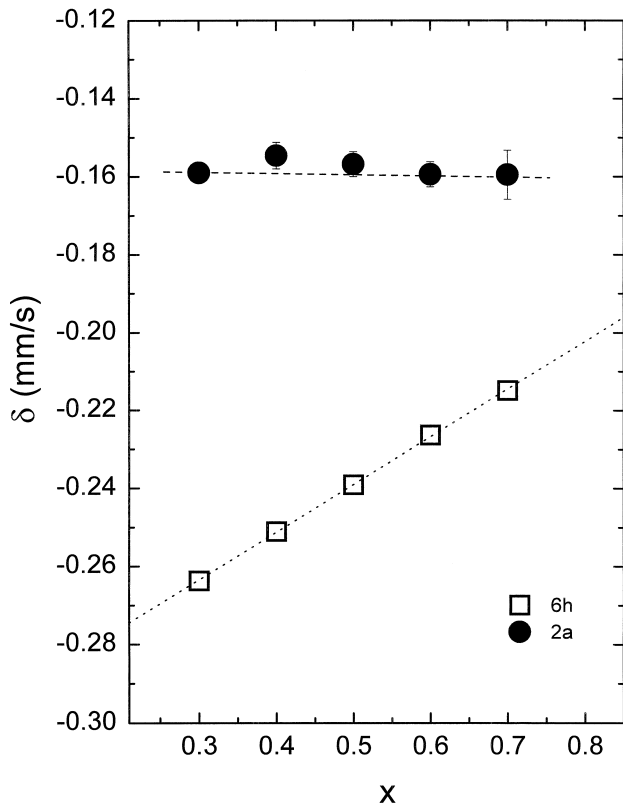


Fig. 8. Experimental isomer shifts of $Zr(Fe_xCr_{1-x})_2$. Dashed lines are linear fits.

populate the transition-metal 3d band, thus reducing the *s*-electron density at the Fe nucleus through a screening effect. On the other hand, the different behavior of the two Fe sites with respect to charge transfer effects may well be related to their different sizes; it would be of interest to investigate this point by means of electronic structure calculations.

As a final remark, we note the two Fe sites in hexagonal $Zr(Fe_xCr_{1-x})_2$ were not resolved in the Mössbauer study of Ref. [5], so the hyperfine parameters quoted therein are average values at best. In a recent paper by Sawicki [18], Mössbauer spectroscopy was used to characterize the metallurgical state of Fe in Zircaloy alloys of use in the nuclear industry. It was found that $Zr(Fe_xCr_{1-x})_2$ compounds appear as precipitates in these alloys, and in one case the measured spectrum was interpreted as a mixture of C14 and C15 phases. According to our present results, however, the spectrum shown would rather be consistent with a single C14 phase. This example stresses the importance of an accurate knowledge of hyperfine parameters if the Mössbauer technique is to be used for materials characterization.

3.2.2. Hydrides

Fig. 9 shows the Mössbauer spectra of the $Zr(Fe_xCr_{1-x})_2H_n$ samples. These spectra could also be fitted with two quadrupolar doublets in the 3:1 ratio, with the exception of $Zr(Fe_{0.7}Cr_{0.3})_2H_{2.5}$, which required an additional pair of doublets amounting to 35% of the total absorption. The latter can be ascribed to the hydrogen-poor α phase. Its spectral area agrees well with the 30% fraction determined by X-ray diffraction. For the other hydrides the α -phase fraction was too small to significantly affect the spectrum fitting and was ignored. It can be noticed that the quadrupolar splittings are greatly enhanced with respect to the unhydrided alloys, reflecting the local symmetry reduction induced by interstitial hydrogen.

In fitting the hydride spectra, the same kind of ambiguity was found as previously described for the alloys. Point-charge calculations would be of little help here due to the additional complication introduced by interstitial hydrogen. A choice was made, instead, based on the following argument. As already mentioned, only A2B2-type interstices are occupied by hydrogen in this system. Most of these tetrahedra have two Zr and two 6h Fe/Cr atoms at their corners, except for the 24l ones which involve one 6h and one 2a-type corner. Thus, 6h Fe atoms are more likely, on the average, to be perturbed by a nearby H than 2a atoms, and one should expect the corresponding Δ to be larger for the former. Thus, the inequality $\Delta(6h) > \Delta(2a)$ was adopted for the site assignment for the hydrides. The fitted parameters are summarized in Table 3.

The quadrupolar splitting in the hydrides is expected to exhibit the following trends: to increase with *x* (similar to

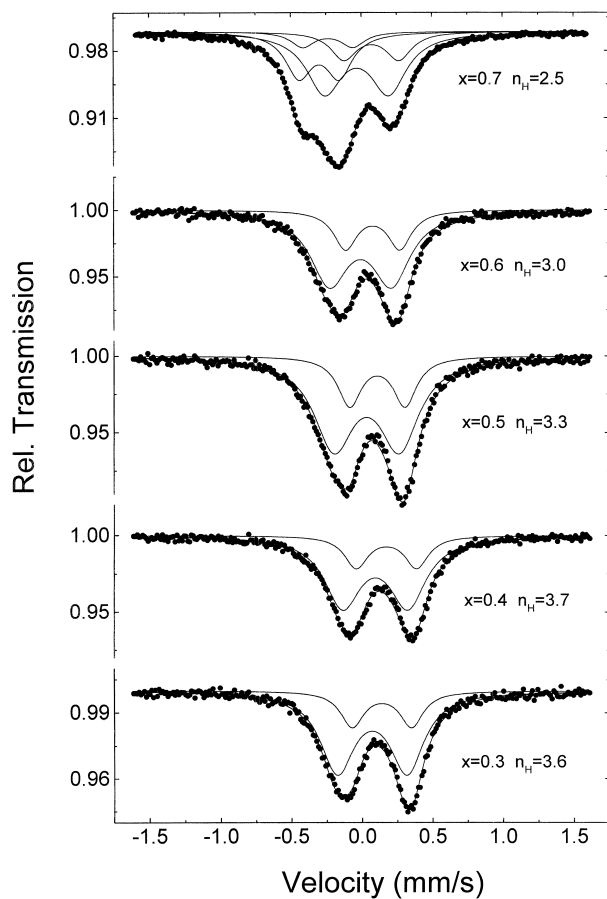


Fig. 9. Room-temperature Mössbauer spectra of $\text{Zr}(\text{Fe}_x\text{Cr}_{1-x})_2\text{H}_n$ hydrides fitted with two doublets in the 3:1 ratio (four doublets for $x=0.7$; see text).

the alloys) due to the charge difference between Fe and Cr, and to increase with n_{H} due to the electrostatic perturbation by H incorporated into the lattice (the concomitant volume expansion should produce the opposite effect, but to a much smaller extent). Since the H absorption capacity in the $\text{Zr}(\text{Fe}_x\text{Cr}_{1-x})_2$ system decreases for increasing Fe concentration, these trends oppose each other. As our data reveal, the effect of hydrogen is the dominant one: Δ decreases for increasing x at both Fe sites, and the increment in Δ due to H absorption is an increasing function of n_{H} , irrespective of x .

As for the isomer shift, all measured values change from negative to positive upon H uptake, as occurs for many metallic systems. The δ increase is plotted as a function of n_{H} in Fig. 10. The behavior is very nearly linear and site-independent. The major cause of the increase in δ is the lattice expansion; an estimate for this contribution, using the experimental expansion vs. n_{H} ratio, is shown by the full line in Fig. 10. It can be seen to account for no more than 66% of the observed effect. In order to explain the excess isomer shift increase, also observed in other hydride systems, it has been suggested [19] that 4s electron states at the Fe site are depleted to fill up a low-lying

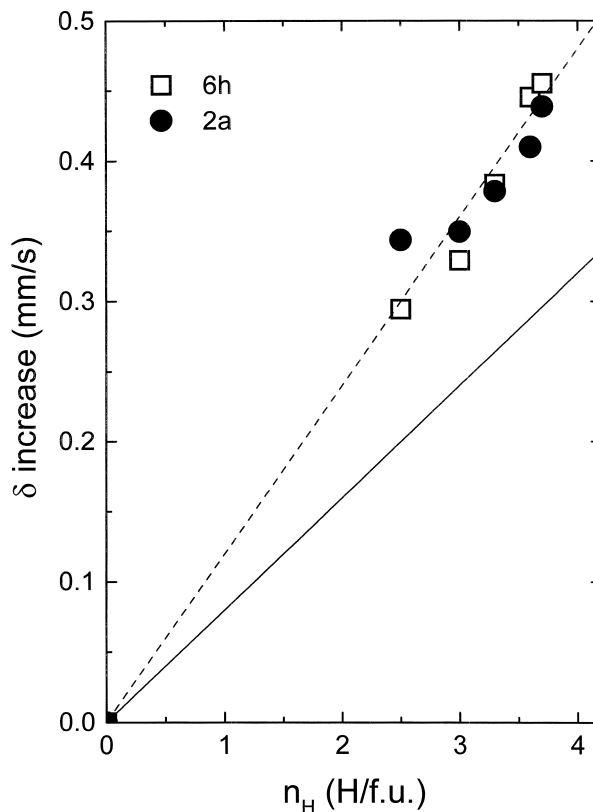


Fig. 10. Isomer shift increase versus absorbed hydrogen amount. Full straight line is calculation based on volume expansion only.

energy band formed through metal–hydrogen bonding, thus lowering the electronic density at the Fe nucleus.

4. Conclusions

We have measured X-ray diffractograms and Mössbauer spectra of $\text{Zr}(\text{Fe}_x\text{Cr}_{1-x})_2$ alloys with the hexagonal C14 structure ($0.3 \leq x \leq 0.7$), as well as of the corresponding hydrides. The two possible Fe sites have been resolved in the Mössbauer spectra. The following trends have been observed for the alloys as a function of increasing Fe concentration: (a) the cell volume decreased at the rate $dV/dx = -11.6 \text{ \AA}^3$; (b) the quadrupole splitting Δ increased at both Fe sites, reflecting a significant charge difference between Fe and Cr atoms; (c) the isomer shift δ increased for 6h-site Fe and was nearly constant for 2a site Fe, in contrast to the decrease to be expected if the volume contraction were to be the dominant effect. In addition, the X-ray data showed the 2a site radius to be 0.6% larger than the 6h one; this difference is likely to be related to the difference in δ vs. x behavior between the two sites.

The hexagonal structure was conserved after hydrogen uptake. The lattice volume expansion was proportional to the absorbed H amount, which ranged from 3.7 to 2.5 H/f.u., decreasing for increasing Fe concentration. Quad-

rupole splittings were larger, and isomer shifts became positive, for the hydrides as compared to the alloys. The measured isomer shift increase was larger than could be explained by volume expansion, suggesting charge transfer effects to be important in these materials.

Acknowledgements

This work was financially supported by FAPESP and CNPq.

References

- [1] D. Shaltiel, I. Jacob, D. Davidov, *J. Less-Common Met.* 53 (1977) 117.
- [2] G. Wiesinger, *J. Magn. Magn. Mater.* 25 (1981) 152.
- [3] I. Nowik, I. Jacob, R. Moreh, *Phys. Rev. B* 47 (1993) 723.
- [4] G. Wiesinger, *Hyperfine Int.* 28 (1986) 545.
- [5] F. Labenski de Kanter, C. Saragovi-Badler, M. Granovski, D. Arias, in: E. Baggio-Saitovitch, E. Galvão da Silva, H.R. Rechenberg (Eds.), *Applications of the Mössbauer Effect*, World Scientific, Singapore, 1990, p. 246.
- [6] K. Kanematsu, *J. Phys. Soc. Jpn.* 29 (1970) 864.
- [7] J.C. Taylor, C.E. Matulis, *J. Appl. Crystallogr.* 24 (1991) 14.
- [8] O. Canet, M. Latroche, F. Bourée-Vignerol, A. Percheron-Guégan, *J. Alloys Compd.* 210 (1994) 129.
- [9] J. Mestnik Filho, A.W. Carbonari, W. Pendl Jr., J.I. Moura, R.N. Saxena, *J. Alloys Compd.* 224 (1995) 60.
- [10] J.A.H. Coaquira, PhD thesis, São Paulo University, 1998.
- [11] K. Kanematsu, *J. Phys. Soc. Jpn.* 27 (1969) 849.
- [12] P. Villars, L.D. Calvert (Eds.), *Pearson's Handbook of Crystallographic Data for Inter-metallic Phases*, The Materials Information Society ASM-International, USA, 1991, p. 3879.
- [13] D.P. Shoemaker, C.B. Shoemaker, *J. Less-Common Met.* 68 (1979) 43.
- [14] D. Ivey, D. Northwood, *J. Less-Common Met.* 115 (1986) 23.
- [15] D. Fruchart, A. Rouault, C.B. Shoemaker, D.P. Shoemaker, *J. Less-Common Met.* 73 (1980) 363.
- [16] D.G. Westlake, *J. Less-Common Met.* 90 (1983) 251.
- [17] D.L. Williamson, in: G.K. Shenoy, F.E. Wagner (Eds.), *Mössbauer Isomer Shift*, North-Holland, Amsterdam, 1978.
- [18] J.A. Sawicki, *J. Nucl. Mater.* 228 (1996) 238.
- [19] M. Gupta, *Solid State Commun.* 42 (1982) 501.